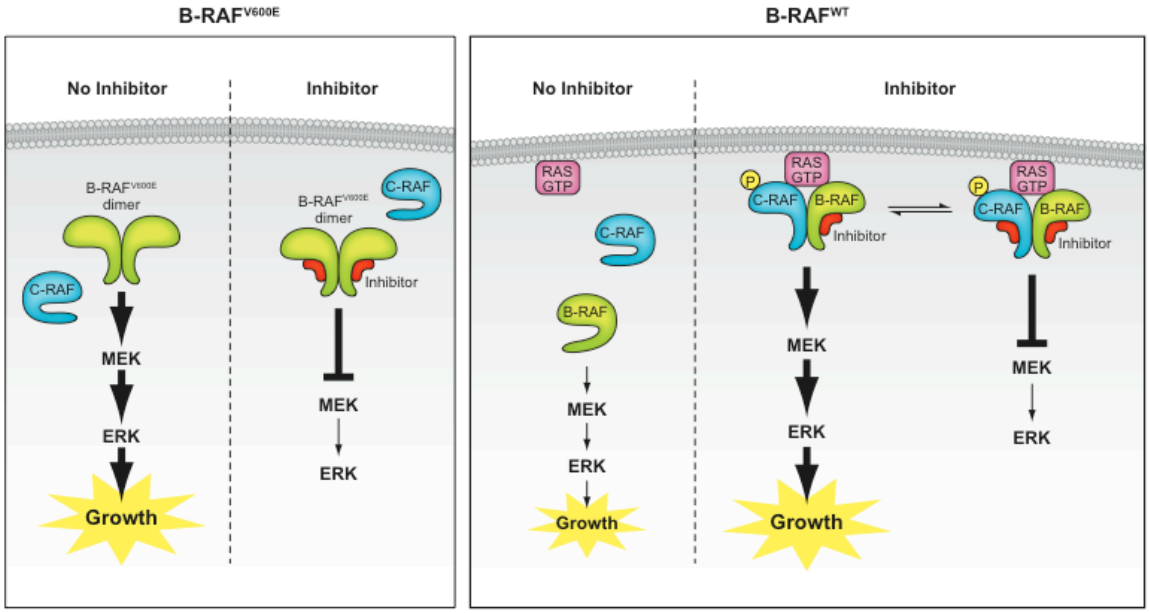

Supplementary Figure 1. Model depicting the mechanism of action of RAF inhibitors in a B-RAF^{V600E} versus B-RAF^{WT} genetic background. In B-RAF^{V600E} cells, the pathway is sensitized to ATP-competitive RAF inhibitors due to the higher ATP $K_{m(app)}$ of the mutant B-RAF^{V600E} protein (Supplementary Fig. 4). Furthermore, there is no discernable induction of phospho-MEK or phospho-ERK in B-RAF^{V600E} cells since: a) inhibitors do not initiate the C-RAF activation sequence and b) signaling to MEK is dominated by B-RAF^{V600E}, with other RAF isoforms playing a lesser role[1,2]. Therefore, RAF inhibitors effectively block signaling and decrease tumor growth in B-RAF^{V600E} tumors. In B-RAF^{WT} cells, inhibitor binding induces wildtype RAF isoform heterodimer and homodimer formation, membrane localization, phosphorylation and activation in a RAS-GTP dependent manner. In a subset of non-B-RAF^{V600E} lines and in some normal tissue, this can lead to enhanced growth depending on cellular context, suggesting that additional signals are required for priming to generate a hyper-proliferative response. The ability of primed C-RAF to signal downstream to MEK depends on: a) inhibitor concentration, b) inhibitor potency against C-RAF and c) inhibitor off-rate. As an example, the irreversible, potent C-RAF inhibitor AZ-628 promotes priming but also blocks phospho-MEK induction through persistent occupancy of the ATP binding pocket. On the other hand, GDC-0879 with a rapid off-rate and intermediate C-RAF potency blocks phospho-MEK induction only at high concentrations. The induction of C-RAF homodimers in the cytosol (by PLX4720) should follow these principles: signaling to MEK occurs when one of the C-RAF protomers within the dimer is not occupied with inhibitor. Homodimer formation is discussed in the main text and is omitted from the model for clarity.

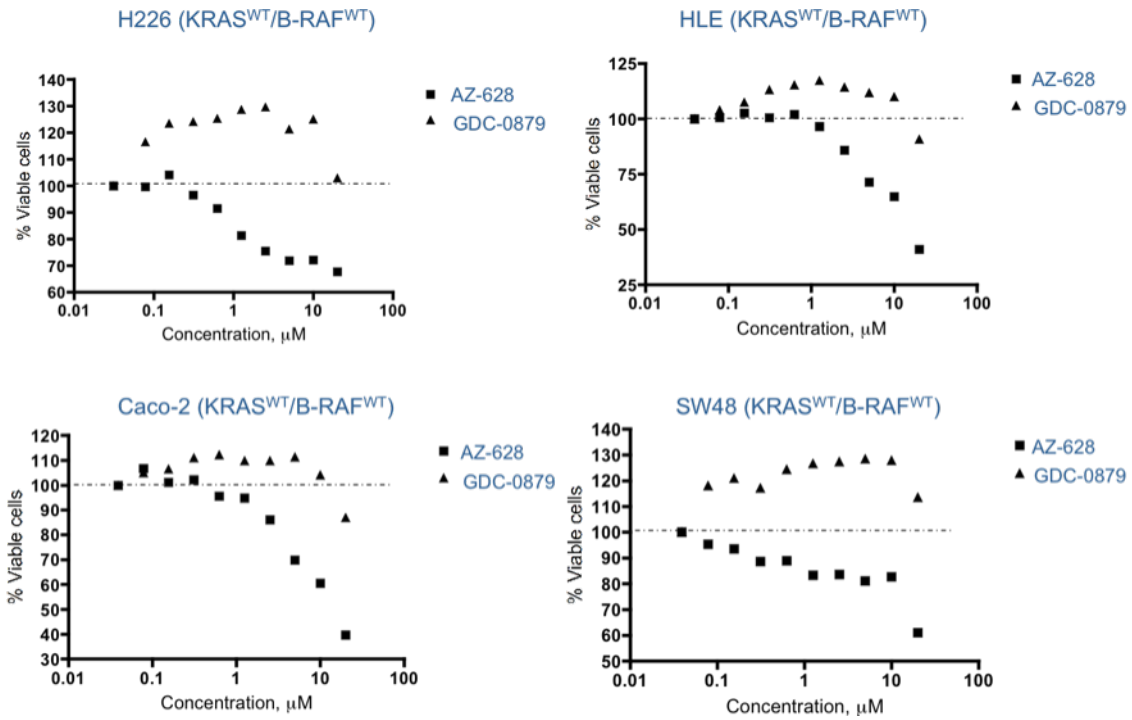

Supplementary Figure 2. Four-day proliferation curves of RAS^{WT}/RAF^{WT} cells upon treatment with GDC-0879 show induction of viable cell counts. In contrast, treatment with AZ-628 induces a reduction in viable cell counts.

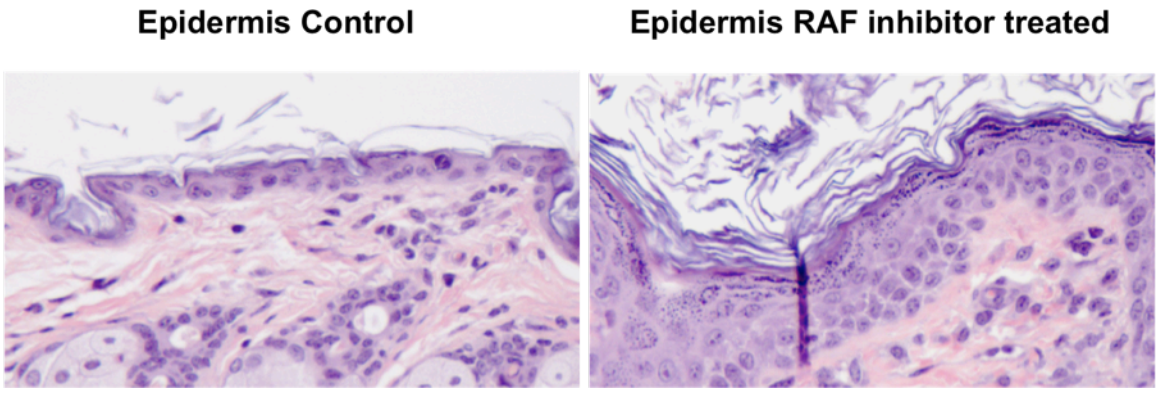

Supplementary Figure 3. Hematoxylin and eosin staining of skin samples from mice treated with vehicle or 100 mg/kg GDC-0879 (po). GDC-0879 treated mice develop hyperkeratosis, acanthosis of the epidermis, and inflammation in the dermis.

a

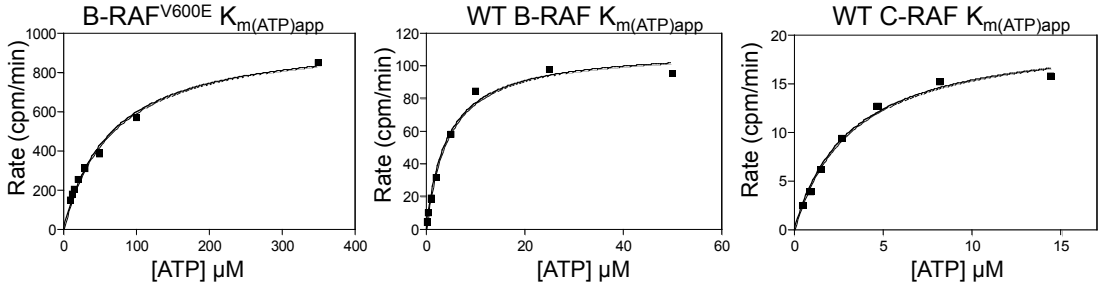

b

Compound	B-RAF^{V600E} $K_{m(ATP)app}$ = 65 µM		WT B-RAF $K_{m(ATP)app}$ = 5 µM		WT C-RAF $K_{m(ATP)app}$ = 3 µM	
	$K_{i(app)}$ (nM)	Adj. IC_{50} (nM) @ 1 mM ATP	$K_{i(app)}$ (nM)	Adj. IC_{50} (nM) @ 1 mM ATP	$K_{i(app)}$ (nM)	Adj. IC_{50} (nM) @ 1 mM ATP
GDC-0879	0.19 ± 0.05	3.2 ± 0.8	0.17 ± 0.02	34 ± 3	0.54 ± 0.04	180 ± 10
PLX4720	4.0 ± 0.8	65 ± 13	2.6 ± 0.4	530 ± 80	3.3 ± 1.9	1100 ± 600

<100 nM >100 nM >500 nM

Supplementary Figure 4. Enzymatic characterization of mutant versus wildtype RAF isoforms and their inhibition by RAF inhibitors. (a) $Km_{(ATP)app}$ determinations for full length B-RAF^{V600E}, B-RAF^{WT}, and C-RAF^{WT}. $Km_{(ATP)app}$ values were determined by fitting a hyperbolic model to the enzymatic rate vs. [ATP] data for B-RAF^{V600E}, B-RAF^{WT}, and C-RAF^{WT}. (b) Table of inhibitor $K_{i(app)}$ and estimated IC_{50} values under cellular ATP concentrations for RAF inhibitors against full-length B-RAF^{V600E}, B-RAF^{WT} and C-RAF^{WT} proteins. $K_{i(app)}$ and predicted IC_{50} values at 1 mM ATP were calculated using the Cheng-Prusoff relationship ($IC_{50} = K_i (1 + S/K_m)$ assuming compounds are competitive with ATP. $K_{i(app)}$ values are represented as mean ± standard deviation ($n \geq 3$). These results show that both GDC-0879 and PLX4720 act as pan-RAF inhibitors in the standard kinase assays, with nearly equal $K_{i(app)}$ for B-RAF^{V600E}, B-RAF^{WT} and C-RAF. However, due to the significantly higher ATP $K_{m(app)}$ for the mutant B-RAF^{V600E} (65 µM) versus the wildtype enzymes (3-5 µM), the wildtype RAF isoforms are predicted to be relatively resistant to RAF inhibitors versus the B-RAF^{V600E} mutant under mM cellular ATP concentrations. This is reminiscent of the situation with wildtype versus activated mutant EGFR isoforms, which are relatively resistant to EGFR inhibitors due to their higher affinity for ATP compared to their mutant counterparts[3, 4].

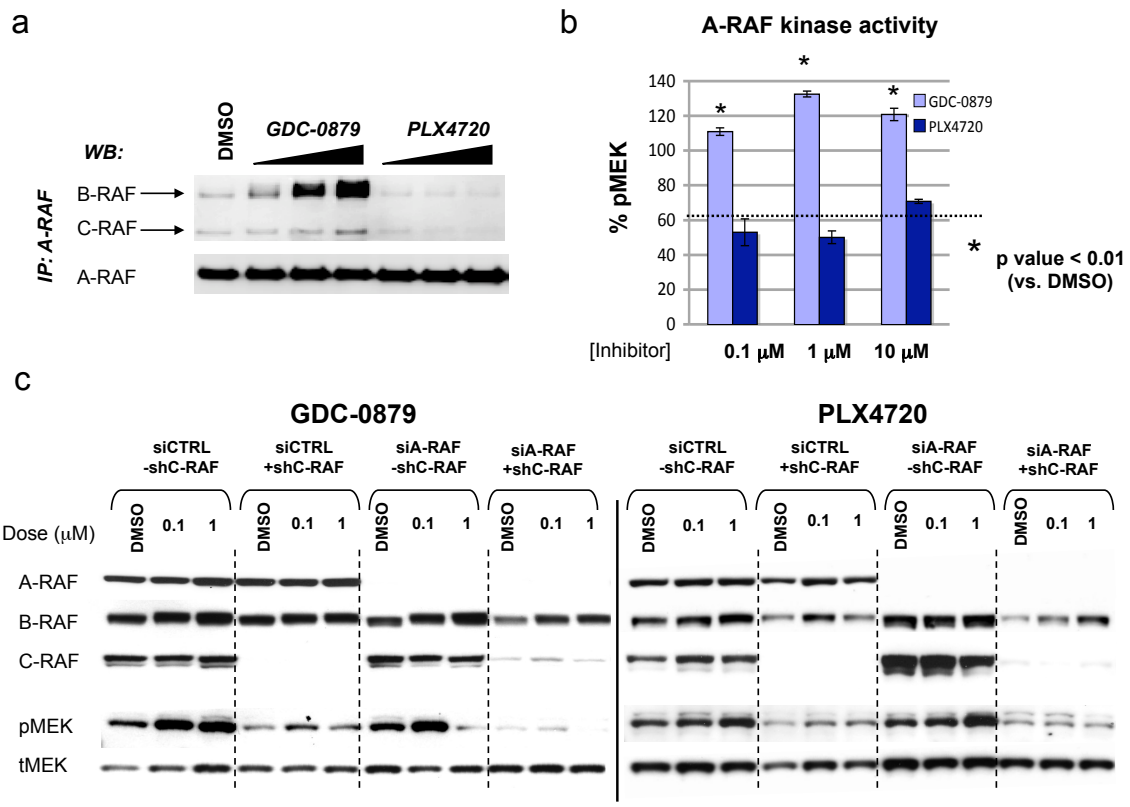

Supplementary Figure 5. Role of A-RAF in inhibitor induced priming of RAF activity (a) A-RAF immunoprecipitated from MeWo cells treated with 0.1, 1, or 10 μM GDC-0879 or PLX4720 demonstrates that A-RAF can form a complex with B-RAF and C-RAF upon treatment with GDC-0879 but not with PLX4720. (b) MeWo cells were treated with GDC-0879 or PLX4720 followed by A-RAF immunoprecipiation and kinase assay. Treatment with GDC-0879 and not PLX4720 induces A-RAF kinase activity. (c) Targeted knockdown of C-RAF (shC-RAF), A-RAF (siA-RAF) or both in GDC-0879 or PLX4720 treated HCT116 cells. Cells lysates were immunobloted for A-RAF, B-RAF, C-RAF, pMEK, and total MEK . Knockdown of both A-RAF and C-RAF has a synergistic effect on decreasing pMEK levels in GDC-0879 treated cells.

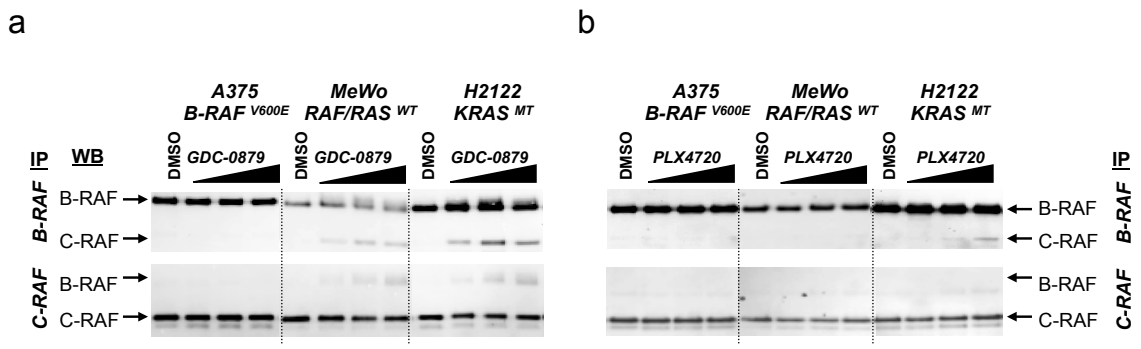

Supplementary Figure 6. Immunoblot of immunoprecipitated (IP) B-RAF or C-RAF shows B-RAF:C-RAF heterodimers in GDC-0879-treated (0.1, 1, 10 μM) MeWo and H2122 cells but not in A375 cells ($B\text{-}RAF^{V600E}$). PLX4720 treatment did not result in heterodimer formation in any of the cell lines tested.

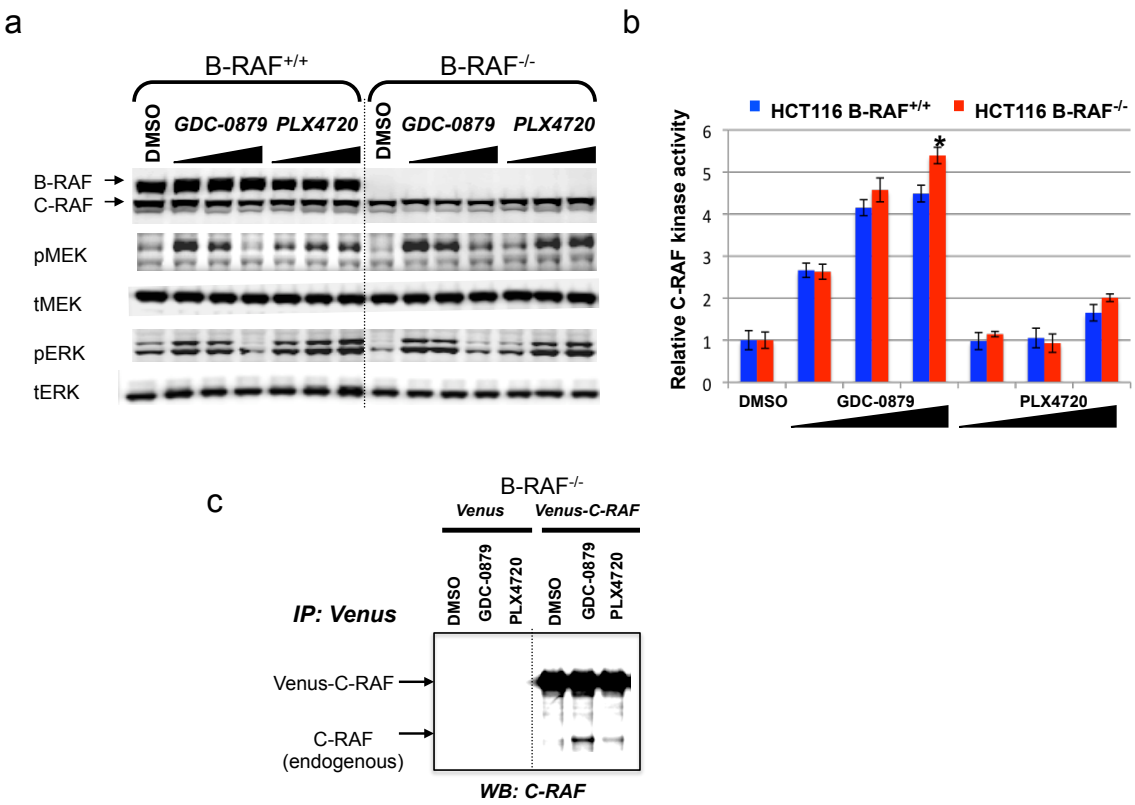

Supplementary Figure 7. RAF/MEK/ERK pathway activation by RAF inhibitors in B-RAF$^{+/+}$ versus B-RAF$^{-/-}$ HCT116 (KRAS^{MT}) cells. (a) Immunoblot for B-RAF, C-RAF, pMEK, total MEK, pERK, and total ERK in HCT116 B-RAF$^{+/+}$ and B-RAF$^{-/-}$ cells treated with 0.1, 1, or 10 μM GDC-0879 or PLX4720 for 1 hour. Data is representative of two independent experiments. (b) C-RAF IPs from HCT116 parental and B-RAF$^{-/-}$ cells treated with GDC-0879 or PLX4720 at 0.1, 1, and 10 μM for 1hour demonstrate induction of C-RAF kinase activity in the absence of B-RAF. Data was normalized to DMSO control for both B-RAF$^{+/+}$ parental and B-RAF$^{-/-}$ cells. Asterisks represent p-values <0.01 calculated using a student's t test. (c) Immunoblot of Venus-tagged C-RAF IP from HCT116 B-RAF$^{-/-}$ cells transiently transfected with Venus-C-RAF or control Venus vector and immunoprecipitated with anti-GFP antibody. Cells were treated with 10 μM of GDC-0879 or PLX4720 for 1 hour.

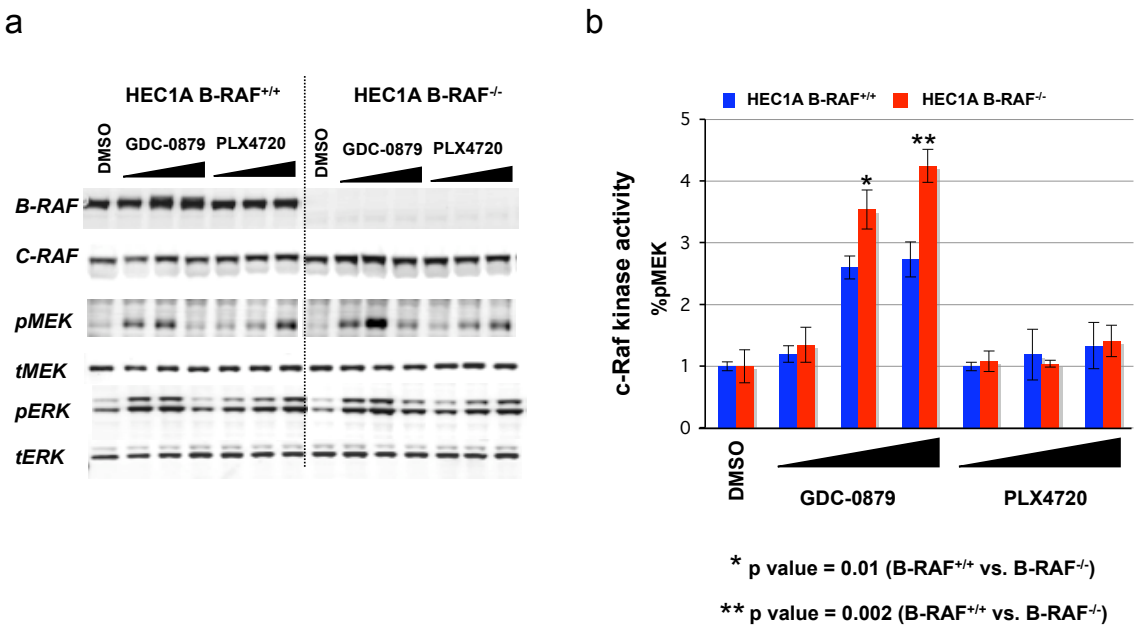

Supplementary Figure 8. RAF/MEK/ERK pathway activation by RAF inhibitors in B-RAF$^{+/+}$ versus B-RAF$^{-/-}$ HEC1A (KRAS^{MT}) cells. (a) HEC1A B-RAF$^{+/+}$ and B-RAF$^{-/-}$ cells treated with 0.1, 1, or 10 μM GDC-0879 or PLX4720 for 1 hour. Cell lysates were immunoblotted for B-RAF, C-RAF, pMEK, total MEK, pERK, and total ERK. (b) C-RAF IP kinase assay from cells treated with 0.1, 1, or 10 μM GDC-0879 or PLX4720. * represents p-values <0.01 and ** <0.002. P values were determined by student's t test. Data is representative of two independent experiments.

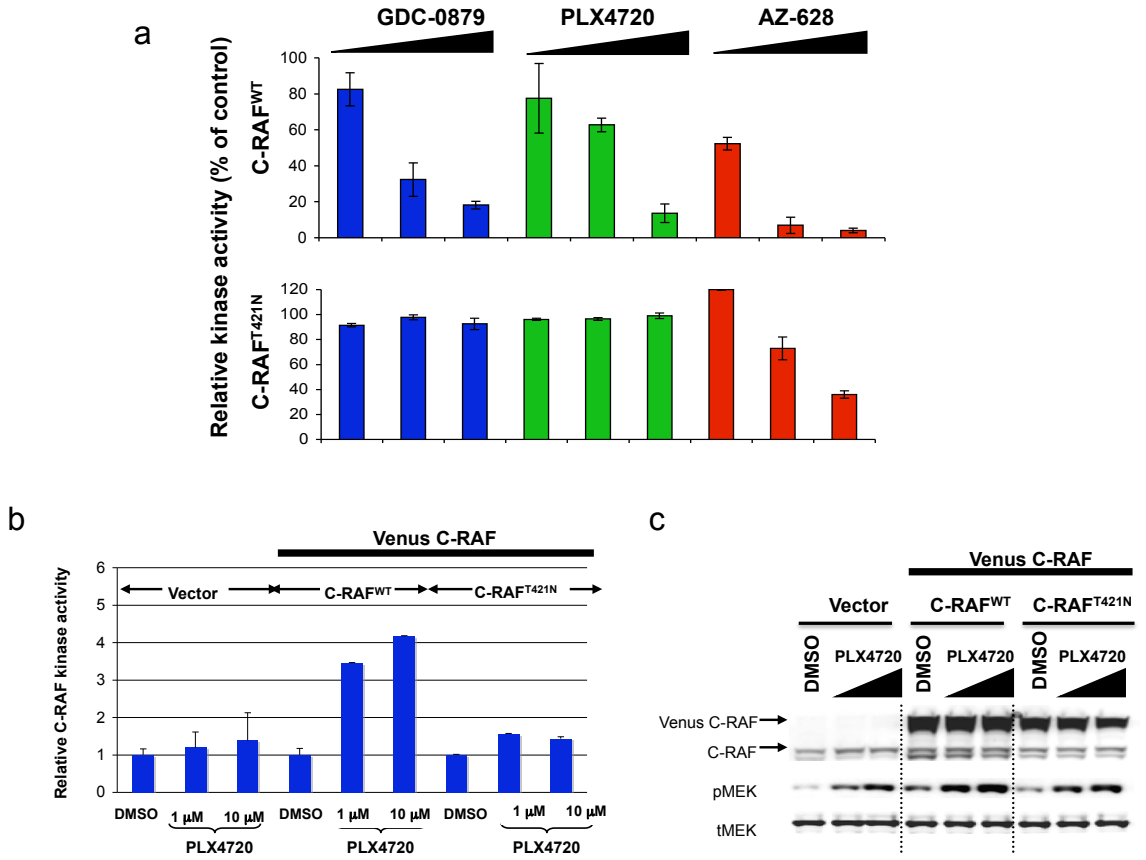

Supplementary Figure 9. Effects of C-RAF^{T421N} gatekeeper mutation on inhibitor binding and cellular effects for PLX4720. (a) HCT116 B-RAF$^{+/+}$ cells were transiently transfected with Venus-C-RAF^{WT} or Venus-C-RAF^{T421N} and C-RAF activity was assayed in an IP kinase assay, using an anti-GFP antibody to pull down exogenous C-RAF and incubating the kinase with 100 μM ATP in the presence of 0.1, 1, and 10 μM of GDC-0879, PLX4720 or AZ-628. GDC-0879 and PLX4720 do not inhibit C-RAF^{T421N} activity and AZ-628 does so moderately. (b,c) HCT116 (KRAS^{MT}) cells transiently transfected with control vector, Venus-C-RAF^{WT} or Venus-C-RAF^{T421N} were treated with 1 and 10 μM of PLX4720 for 1 hour. (b) Venus-tagged C-RAF immunoprecipitated with an anti-GFP antibody was tested in an in vitro kinase assay using recombinant MEK as a substrate. Data was normalized versus DMSO control for each transfection condition. (c) Immunoblot analysis of lysates detected endogenous and over-expressed C-RAF as well as relative phosho-MEK levels under different transfection conditions. All data are representative of at least 2 independent experiments. Error bars represent standard deviation. Binding to the C-RAF nucleotide binding pocket is required for C-RAF activation and phospho-MEK induction as PLX4720 no longer induces RAF kinase activity or pMEK levels upon overexpression of C-RAF^{T421N} in contrast to C-RAF^{WT}.

a

B-RAF^{V600E} Km(ATP)app=65μM	WT B-RAF Km(ATP)app=5μM	WT C-RAF Km(ATP)app=3μM
8.3 nM	220 nM	28 nM

b

Compound	B-RAF^{V600E} Reversibility of Binding	$t_{1/2}$ (min)
GDC-0879	Rapid	<1
PLX4720	Rapid	<1
AZ-628	Very slow or irreversible	>90

c

CELL LINE	GENOTYPE	EC_{50} (μM)
COLO205	B-RAF^{V600E}	0.1
A375	B-RAF^{V600E}	0.08
624	B-RAF^{V600E}	0.16
CaCo-2	RAS/RAF^{WT}	20
H226	RAS/RAF^{WT}	5.8
MeWo	RAS/RAF^{WT}	2.9
HLE	RAS/RAF^{WT}	20
A549	KRAS^{MT}	12

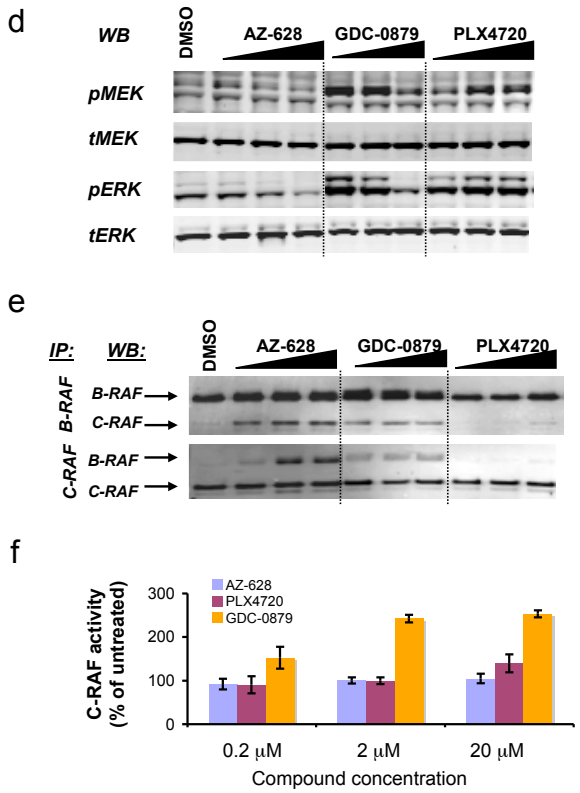

Supplementary Figure 10. Characterization of the AZ-628 RAF inhibitor. (a) Predicted IC50 values at 1 mM ATP for full length B-RAF^{V600E}, B-RAF^{WT}, and C-RAF^{WT} calculated using the Cheng-Prusoff relationship (IC50 = Ki (1 + S/Km) assuming AZ-628 is competitive with ATP. (b) Table of $t_{1/2}$ and reversibility of binding for B-RAF^{V600E} for GDC-0879, PLX4720 and AZ-628. (c) EC_{50} values (μM) in cellular proliferation assays of AZ-628 against a panel of B-RAF^{V600E}, RAS/RAF^{WT} and RAS^{MT} cell lines. (d) MeWo cells treated with 0.2, 2, 20 μM of the indicated RAF inhibitor. Cell lysates were immunoblotted for B-RAF, C-RAF, pC-RAF^{S338}, pMEK, total MEK, pERK and total ERK. (e) B-RAF or C-RAF immunoprecipitated from MeWo cells treated with 0.2, 2, or 20 μM of the indicated Raf inhibitor for 1 hour. Samples were immunoblotted for B-RAF and C-RAF. (f) C-RAF IP kinase assays for MeWo cells treated with 0.2, 2, or 20 μM of the indicated RAF inhibitors for 1hour.

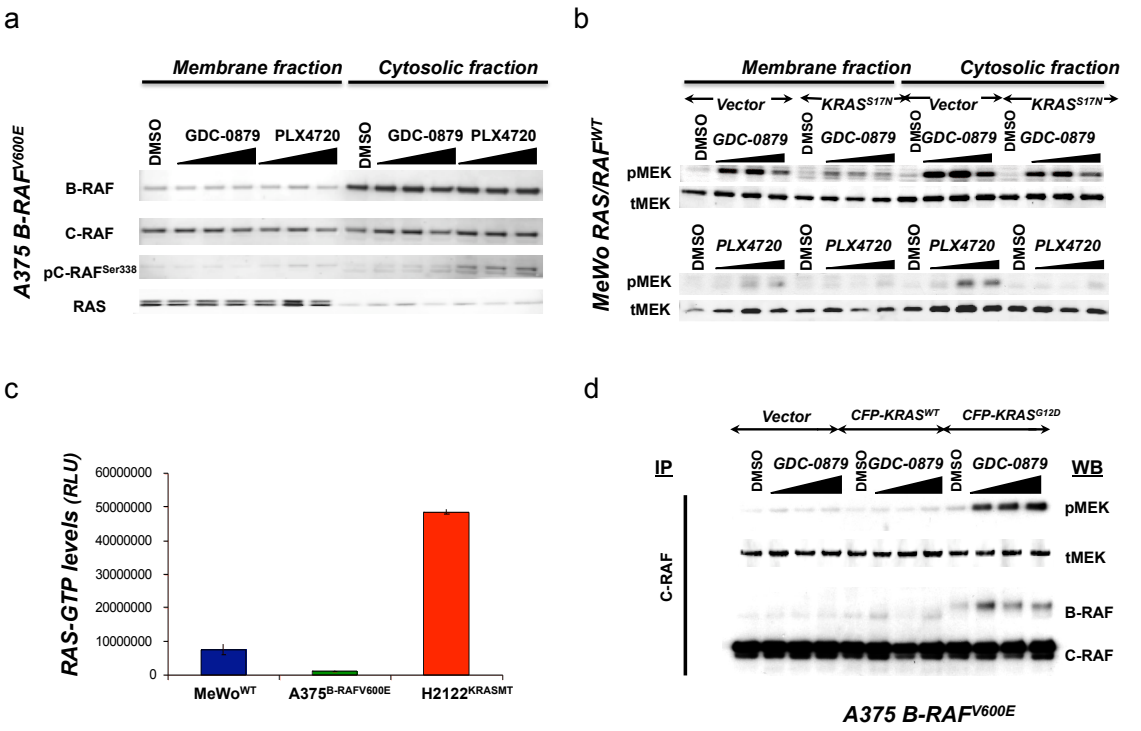

Supplementary Figure 11. Active RAS plays an important role in C-RAF activation and phospho-MEK induction by RAF inhibitors. (a) A375 (B-RAF^{V600E}) cells were treated with GDC-0879 or PLX4720 for 1hour and lysed in hypotonic buffer for membrane fractionation. Both membrane (P100) and cytosolic (S100) fractions were immunoblotted with the indicated antibodies. (b) MeWo cells were transiently transfected with KRAS^{WT} or KRAS^{S17N}, treated with GDC-0879 or PLX4720 (at 0.1, 1, 10 μM) for 1hour and fractionated into membrane (P100) and cytosolic (S100) fractions. Aliquots of the membrane and cytosolic fractions were immunoblotted with anti-phospho- and anti-total MEK antibodies. (c) RAS-GTP levels were measured from lysates of MeWo (RAS/RAF^{WT}), A375 (B-RAF^{V600E}) and H2122 (KRAS^{MT}) cells with a Ras-GTP ELISA protocol using immobilized C-RAF-RBD as bait for capturing RAS-GTP. Relative luminescent units represent RAS detection of an anti-RAS antibody bound to the RBD. RAS-GTP H2122>>Mewo>A375. (d) Transfection of mutant KRAS^{G12D} (but not KRAS^{WT}) in A375 (B-RAF^{V600E}) cells, allows the cells to induce B-RAF:C-RAF heterodimers and C-RAF kinase activation in the presence of the RAF inhibitor GDC-0879 (dosed at 0.1, 1, 10 μM). C-RAF was immunoprecipitated from control and inhibitor-treated cells and assayed for protein activity and B-RAF heterodimerization. Total C-RAF levels shown by WB in the immunoprecipitate indicate loading for each lane.

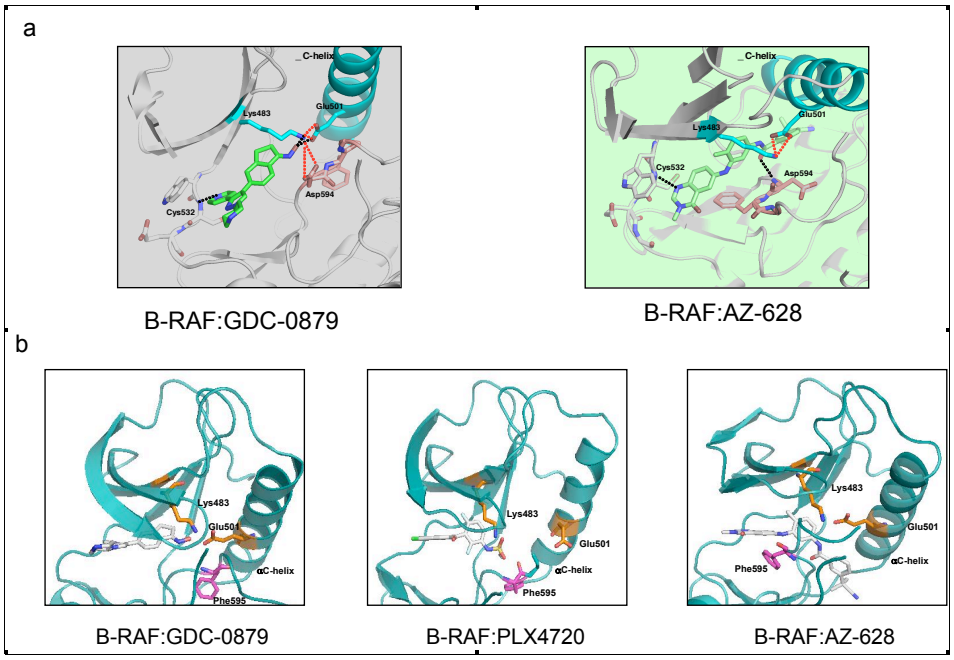

Supplementary Figure 12. GDC-0879, PLX4720 and AZ-628 have distinct binding modes to B-RAF. (a) Comparison of GDC-0879 and AZ-628 hydrogen bond (H-bond) interactions with B-RAF. DFG motif is shown in magenta. The αC-helix, Glu501 on the αC-helix, and the catalytic Lys483 are shown in cyan. The close proximity of Glu501 and Lys483 side chains indicates a salt bridge. Black dotted lines represent H-bond contacts of inhibitor with key residues of the protein. Red dotted lines represent intramolecular distances for key residues in the enzyme. (Left) GDC-0879:B-RAF crystal structure shows Asp594 side chain in the DFG motif makes key bridging interactions with Glu501 and Lys483. This interaction maintains the side chains of Glu501 and Lys483 in a conformation amenable to H-bonding with the highly polarized oxime of GDC-0879. Mutation of Asp594 to alanine would be expected to disrupt these bridging interactions and prevent GDC-0879 from binding to B-RAF. (Right) AZ-628:B-RAF model illustrates H-bond contact with the backbone amide of Asp594 within the B-RAF DFG loop (2.8 Å distance to backbone nitrogen of Asp594). Mutation of Asp594 to alanine would be expected to be tolerated, since similar backbone amide contacts with AZ-628 can be maintained. (b) Detailed views of the ATP binding pockets from B-RAF:GDC-0879 analog (left), B-RAF:PLX4720 (middle) and B-RAF:AZ-628 (right) complexes illustrate the different binding modes of each inhibitor[5,6,7]. The AZ-628:B-RAF complex was modeled as described in the methods summary. Phe595 within the DFG motif of the activation segment is shown in magenta. GDC-0879 and PLX4720 bind to the active "Phe-in" B-RAF conformation, while AZ-628 binds to the inactive "Phe-out" conformation. The catalytic Lys-543 and Glu-501 in the αC-helix (both shown in orange) form a salt bridge based on the AZ-628 and GDC-0879-analog complex structures. PLX4720 binding disrupts this ion pairing by dramatically shifting the αC helix. Disruption of this ion pair and displacement of the N-lobe is a signature feature of many inactive kinase structures[8,9,10,11]. In contrast, maintenance of the ion pair by the AZ-628 and GDC-0879 compounds may help orient the αC-helix in an active conformation within the N-lobe of the RAF kinase domains.

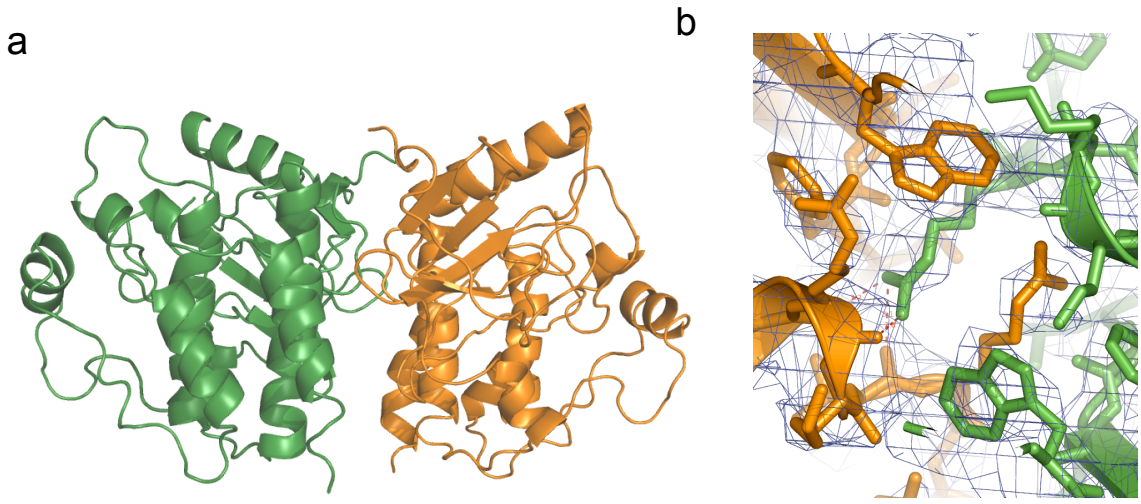

Supplementary Figure 13. Crystal structure of C-RAF homodimer demonstrates a conserved dimer interface. (a) The C-RAF kinase domain crystal structure reveals a side-to-side dimer. The C-RAF kinase domain was co-crystallized with a GDC-0879 analog. The two C-RAF protomers in the asymmetric unit are shown in green and orange ribbons. (b) A view of the C-RAF dimer interface, showing electron density and residues around the key residue Arg401. Monomer A is colored green and monomer B is orange. The $2F_o$- F_c map is contoured at 1σ. Both copies of residue Arg401 lie very close to the two-fold symmetry axis of the C-RAF dimer and are visible in the center of this figure. The guanidium headgroup of A-chain Arg401 appears well positioned to make hydrogen bonds to three carbonyl oxygens in the B-chain: Arg398 (2.8 Å), Thr400 (3.1 Å) and Phe408 (3.3 Å). The B-chain Arg401 appears to make similar interactions with the carbonyl oxygens of Arg398 (3.3 Å) and Leu397 (3.5 Å) in the A-chain.

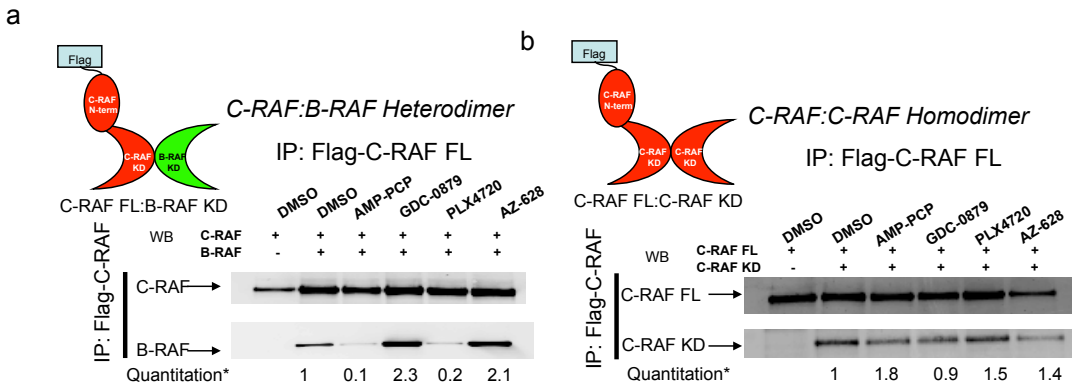

Supplementary Figure 14. B-RAF:C-RAF heterodimerization and not C-RAF homodimerization is dependent on conformation induced by inhibitor binding. (a) Biochemical heterodimerization assay using full length flag-tagged C-RAF and the kinase domain of B-RAF incubated with DMSO, 1 mM AMP-PCP, or 10 μM of inhibitor. Flag-C-RAF full length was immunoprecipiated with anti-flag beads and immunoblotted for C-RAF and B-RAF. GDC-0879 and AZ-628 stabilize the C-RAF:B-RAF heterodimer. (b) Biochemical homodimerization assay using full length flag-tagged C-RAF and kinase domain of C-RAF incubated with DMSO, 1 mM AMP-PCP, or 10 μM of inhibitor. Flag-C-RAF full length was immunoprecipiated with anti-flag beads and immunoblotted for C-RAF and anti-flag. Homodimerization does not appear to be sensitive to conformation induced by inhibitor binding.

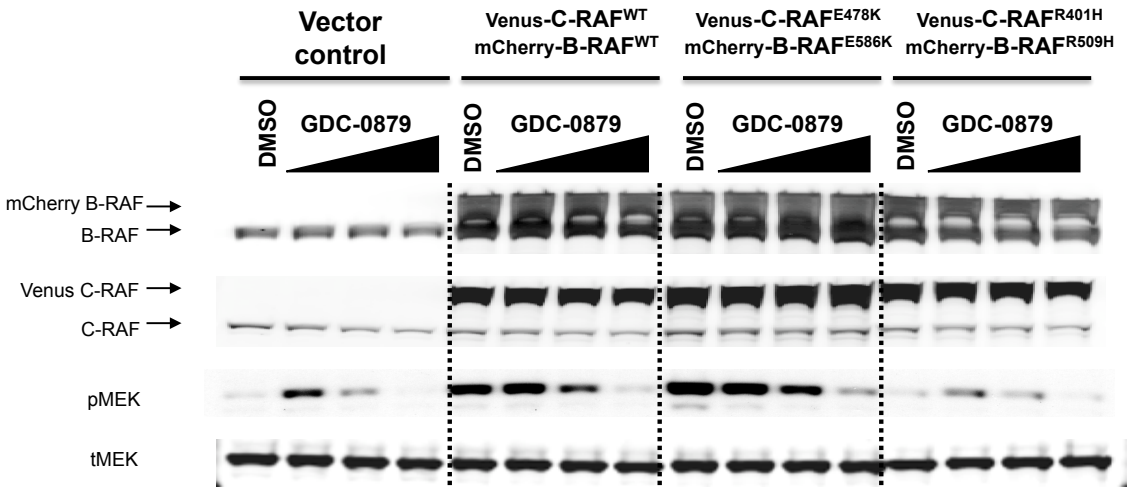

Supplementary Figure 15. C-RAF:B-RAF dimerization is important for pMEK induction. HCT116 (KRAS^{MT}) cells were transiently transfected with the indicated wildtype and dimerization mutant RAF constructs for 48 hours and treated with DMSO or 0.1, 1, 10 μM GDC-0879. Lysates were immunoblotted for B-RAF, C-RAF, pMEK and total MEK. Overexpression of wildtype and dimerization-promoting mutants (Venus-C-RAF^{E478K} and mCherry-B-RAF^{E586K}) increases basal pMEK levels with no further induction upon inhibitor treatment. In contrast, overexpression of the dimerization defective mutants (Venus-C-RAF^{R401H} and mCherry-B-RAF^{R509H}) result in a decrease of basal pMEK levels and severely impaired induction of pMEK levels upon treatment with GDC-0879.

	C-RAF _1
Data collection	
Space group	$P4_12_12$
Cell dimensions	
a, *b*, *c* (Å)	42.08, 86.93, 86.24
α, β, γ (°)	118.11, 99.65, 95.47
Resolution (Å)	30.0-4.0 (4.22 -4.0)
R_{sym}	0.167 (0. 311)
$I / \sigma I$	4.32 (2.50)
Completeness (%)	99.8 (100.0)
Redundancy	13.8 (14.2)
Refinement	
Resolution (Å)	30.0 – 4.0
No. reflections	7341
R_{work} / R_{free}	0.290/0.372
No. atoms	
Protein	4262
Ligand/ion	0
Water	0
B-factors	
Protein	68.0 (Uniform)
Ligand/ion	
Water	
R.m.s. deviations	
Bond lengths (Å)	0.007
Bond angles (°)	1.06

Supplementary Table 1. Crystallographic table for C-RAF crystal structure bound to RAF inhibitor. The crystal was frozen at 100K and data were collected in-house on an FR-E generator and Raxis-IV++ detector (Rigaku) at 1.54A wavelength. Since the crystal only diffracted to 4.0 Å, additional precautions were taken during refinement in Refmac: NCS restraints were enforced on all residues of both chains and a low X-ray weighting term of 0.0025 was used. Also, all atoms were given a fixed isotropic B-factor of 68.0. No water atoms were added to the structure and, although there was weak density visible for the ligand, it was not modeled in. The final structure had reasonably good geometry and in the Ramachandran plot of the final structure only 8/468 residues (1.7%) are in disallowed regions.

B-RAF Residue		Buried Surface Area	C-RAF Residue		Buried Surface Area
Number	**Name**	**(Angstroms^2)**	**Number**	**Name**	**(Angstroms^2)**
448	**ASP**	82.8	340	**TYR**	66.6
450	TRP	68.9	342	TRP	79.8
476	TRP	28.0	368	TRP	30.5
477	HIS	117.0	369	HIS	131.5
478	GLY	18.5	370	GLY	19.6
506	ARG	43.2	398	ARG	55.5
507	LYS	51.1	399	LYS	71.1
509	ARG	180.0	401	ARG	206.5
510	HIS	46.6	402	HIS	42.3
511	VAL	61.8	403	VAL	67.2
515	LEU	58.3	407	LEU	87.1
516	PHE	18.2	408	PHE	24.1
517	MET	48.3	409	MET	45.5
562	GLN	39.1	454	GLN	37.4
565	ASP	13.1	457	ASP	16.5
566	TYR	41.8	458	TYR	41.0
569	ALA	22.2	461	ALA	16.0
570	LYS	41.4	462	LYS	39.4
585	HIS	13.8	477	HIS	17.4
586	GLU	33.8	478	GLU	19.3
588	LEU	47.2	480	LEU	39.2
589	THR	12.2	481	THR	8.6

Supplementary Table 2. B-RAF and C-RAF dimer interface comparison. Residues that bury >10 Å^2 in the crystallographic dimer interface are listed. The only residue difference in the interface is a regulatory residue, C-RAF^{Y340}, compared with B-RAF^{D448}. Solved-accessible areas were calculated with the program "Surface" from the CCP4 suite, using a probe radius of 1.4 Å.

Supplementary References

1 Pratilas, C. A. et al., (V600E)BRAF is associated with disabled feedback inhibition of RAF-MEK signaling and elevated transcriptional output of the pathway. *Proc Natl Acad Sci U S A* **106** (11), 4519 (2009).

2 Dumaz, N. et al., In melanoma, RAS mutations are accompanied by switching signaling from BRAF to CRAF and disrupted cyclic AMP signaling. *Cancer Res* **66** (19), 9483 (2006).

3 Yun, C. H. et al., Structures of lung cancer-derived EGFR mutants and inhibitor complexes: mechanism of activation and insights into differential inhibitor sensitivity. *Cancer Cell* **11** (3), 217 (2007).

4 Yun, C. H. et al., The T790M mutation in EGFR kinase causes drug resistance by increasing the affinity for ATP. *Proc Natl Acad Sci U S A* **105** (6), 2070 (2008).

5 Wan, P. T. et al., Mechanism of activation of the RAF-ERK signaling pathway by oncogenic mutations of B-RAF. *Cell* **116** (6), 855 (2004).

6 Hansen, J. D. et al., Potent and selective pyrazole-based inhibitors of B-Raf kinase. *Bioorg Med Chem Lett* **18** (16), 4692 (2008).

7 Tsai, J. et al., Discovery of a selective inhibitor of oncogenic B-Raf kinase with potent antimelanoma activity. *Proc Natl Acad Sci U S A* **105** (8), 3041 (2008).

8 Gassel, M. et al., The protein kinase C inhibitor bisindolyl maleimide 2 binds with reversed orientations to different conformations of protein kinase A. *J Biol Chem* **279** (22), 23679 (2004).

9 Zhao, B. et al., Crystal structure of the kinase domain of serum and glucocorticoid-regulated kinase 1 in complex with AMP PNP. *Protein Sci* **16** (12), 2761 (2007).

10 Huang, X. et al., Crystal structure of an inactive Akt2 kinase domain. *Structure* **11** (1), 21 (2003).

11 Smith, K. J. et al., The structure of MSK1 reveals a novel autoinhibitory conformation for a dual kinase protein. *Structure* **12** (6), 1067 (2004).